ACS Sustainable Chemistry & Engineering

Research Article

pubs.acs.org/journal/ascecg

A Unique Silk Mat-Like Structured Pd/CeO_2 as an Efficient Visible Light Photocatalyst for Green Organic Transformation in Water

Yanhui Zhang,[†,‡] Nan Zhang,[†,‡] Zi-Rong Tang,[‡] and Yi-Jun Xu[†,‡,*]

[†]State Key Laboratory Breeding Base of Photocatalysis, College of Chemistry and Chemical Engineering, Fuzhou University, Fuzhou 350002, P. R. China

[‡]College of Chemistry and Chemical Engineering, New Campus, Fuzhou University, Fuzhou 350108, P. R. China

Supporting Information

ABSTRACT: The charm embedded in nature is its inherent power to create a myriad of materials, for example, a spider web and lotus leaf, with ordinary composition but exhibiting fascinating functional property owing to their unique structures. Such intricate natural designs inspire immense research in synthesizing materials with controlled structure and morphology toward achieving novel or enhanced properties for target applications. Herein, we report a rotary vacuum evaporation and support-driven nanoassembly of tiny Pd noble metal particles on nanosized CeO_2, which features a remarkable unique silk "mat-like" morphology with significant anti-aggregation of Pd nanoparticles during a high temperature calcination process, whereas the obvious aggregation phenomenon of Pd nanoparticles occurs when using commercial CeO_2 as a support. This nanocomposite with unique structural and morphology composition is able to act as a highly selective and active visible light photocatalyst toward organic redox transformations in water, including aerobic oxidation of alcohols and anaerobic reduction of nitro-compounds under ambient conditions, representing a typical tenet of photocatalytic green chemistry.

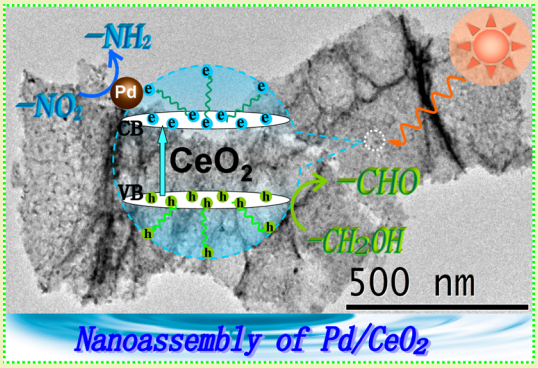

KEYWORDS: *Nanoassembly, Silk mat , CeO_2, Pd nanoparticles, Selective redox, Water*

INTRODUCTION

The capture and conversion of solar energy by semiconductor-based heterogeneous photocatalysis has gained immense attention by the scientific and engineering world because of the great potential in resolving energy and environmental issues toward sustainable processes, for example, degradation of organic pollutants or bacteria, photoreduction of CO_2 to solar fuels, and photocatalytic water splitting.[1−5] The optimization and manipulation of charge carrier transfer processes on semiconductor surfaces are a key and broad theme for improving the efficiency of such semiconductor-based artificial photosynthesis.[1−10] In addition, many microscopic structural and morphology factors, e.g., size, shape, crystal facet, promoter, or localized compositional variation of a specific semiconductor-based photocatalyst, together have synergistic and significant impacts on the overall performance of photocatalysts, including tuning the activity and selectivity to specific products.[11−20] Thus, structure- and morphology-dependent photocatalysis has been a general versatile rationale for tuning the photocatalytic activity/selectivity for a specific semiconductor independent of what kinds of reactions are targeted.[11−15,18−22] Research interest in our laboratory is primarily focused on the synthesis or discovery of semiconductor-based materials with specific architectural structure/morphology toward photocatalytic "selective" organic redox transformation to fine chemicals.[13,15]

Selective oxidation is important in the synthesis of fine chemicals and intermediates. In particular, selective oxidation of alcohols to corresponding carbonyl (adehydes or ketones) compounds represents one important organic transformation because carbonyl compounds are widely used as valuable intermediates in the fragrance, confectionary, and pharmaceutical industries.[16,17,23−27] Many oxidations of this type are carried out using stoichiometric oxygen donors such as chromate or permanganate, but these reagents are expensive and have serious toxicity issues associated with them.[24,26,28−30] Thus, heterogeneous photocatalytic selective oxidation of alcohols using O_2 molecules at room temperature has been proposed as an attractive environmentally benign method for organic synthesis.[28−32] Although photocatalytic selective oxidation of organic compounds has been difficult because of the strong oxidation power resulting from photogenerated holes and active oxygen species (e.g., superoxide radicals), recent progress on aerobic selective oxidation of alcohols to carbonyl compounds over TiO_2-based semiconductors, graphene-semiconductor nanocomposites, and plasmonic Au metal photocatalysts highlights that the rational use of appropriate semiconductors and fine control of reaction

Received: April 23, 2013
Revised: July 10, 2013
Published: July 11, 2013

conditions can promote organic reactions to occur with high selectivity and activity.[17,23−25,33−36] For example, Palmisano and co-workers demonstrated that in water a homemade rutile TiO_2 with bad crystallinity can exhibit a moderately high selectivity for oxidation of aromatic alcohols to aldehydes in water under UV light irradiation.[17] These encouraging results suggest that in the presence of holes and active oxygen species (e.g., superoxide and hydroxyl radicals) the selectivity for aerobic photocatalytic oxidation of alcohols can be flexibly tuned by controlling other structural/morphology factors. Thus, it is clear that there is still a wide scope to synthesize and explore semiconductor-based photocatalysts featuring specific structural and morphological composition toward selective oxidation of alcohols and other important organic transformations in water.

Toward this purpose, we herein report a rotary vacuum evaporation and support-driven synthesis of tiny noble metal Pd nanoparticles on the nanosized CeO_2 support (denoted as Pd/CeO_2−NPs) with an unexpected unique silk "mat-like" morphology. In sharp contrast, when using commercial CeO_2 powder as support instead of nanosized CeO_2 powder, this remarkable morphology can not be formed; besides, the Pd nanoparticles undergo the obvious aggregation, which is not observed for Pd/CeO_2−NPs. Because the CeO_2-supported noble metal nanoparticles have shown unique catalytic performances for oxidations originated from the synergistic effects between the support and metal nanoparticles, Pd/CeO_2 was selected as the subject of this investigation. Importantly, such a nanoassembly of Pd/CeO_2−NPs with unique mat morphology can act as an efficient visible light-driven photoactive and highly selective catalyst for aerobic oxidation of alcohols and anaerobic reduction of nitro-compounds in water as a green solvent under ambient conditions, i.e., room temperature and atmospheric pressure.

■ EXPERIMENTAL SECTION

Materials. Nanosized CeO_2 powder (CeO_2−NPs, average particle size 15−30 nm) is supplied from Alfa Asear. Commercial CeO_2 powder (average particle size 50−500 nm), polyvinylpyrrolidone (PVP, MW: 40 000), andydrous ethanol, and $PdCl_2$ are supplied from Sinopharm Chemical Reagent Co., Ltd. (Shanghai, China). All of the chemicals are analytic grades and used as received. Deionized water is supplied from local resources.

Synthesis. Synthesis of homogeneous PVP-capped noble metal Pd colloidal solution was performed by the alcohol reduction method.[37,38] First, the H_2PdCl_4 aqueous solution (2.0 mM) was prepared by dissolving the precursor $PdCl_2$ into HCl aqueous solution. Then, a mixture of the above H_2PdCl_4 solution (15 mL), 21 mL of H_2O, 14 mL of ethanol, and 0.0667 g of PVP was refluxed at 363 K for 3 h with stirring. The resulting brown solution of Pd colloids protected by PVP was obtained, which is stable for months at room temperature. The synthesis of Pd/CeO_2−NPs was done as following: 0.1277 g of CeO_2−NPs was added to the calculated amount of the above Pd colloids to prepare 5 wt % Pd/CeO_2−NPs composites. The mixing solution was aged with vigorous stirring for 24 h to obtain a homogeneous suspension. Then, this suspension was evaporated in a rotary evaporator in vacuum in a water bath at 323 K and then fully dried at 373 K in an oven. Followed by calcination at 673 K in air for 2 h, the final Pd/CeO_2−NPs was obtained. The synthesis of Pd/commercial CeO_2 was done using the same preparation procedure as that for Pd/CeO_2−NPs except that CeO_2−NPs were replaced by commercial CeO_2.

Characterizations. The optical properties of the samples were analyzed using a UV−vis spectrophotometer (Cary-500, Varian Co.) in which $BaSO_4$ was used as the background. The Brunauer−Emmett−Teller (BET) specific surface area of the samples was analyzed by nitrogen adsorption in a Micromeritics ASAP 2020 apparatus. SEM images were obtained by field emission scanning electron microscopy (SEM) on a FEI Nova NANOSEM 230 spectrophotometer. TEM images were obtained using a JEOL model JEM 2010 EX instrument at an accelerating voltage of 200 kV. X-ray photoelectron spectroscopy (XPS) measurements were performed using a Thermo Scientific ESCA Lab250 spectrometer, which consists of a monochromatic Al Kα as the X-ray source, hemispherical analyzer, and sample stage with multi-axial adjustability to obtain the composition on the surface of samples. All of the binding energies were calibrated by the C 1s peak at 284.6 eV. The photoluminescence (PL) spectra were performed on an Edinburgh FL/FS900 spectrophotometer. In particular, for the measurement of hydroxyl radicals by the reaction with teraphthalic acid (TA) as a probe molecule, the as-prepared catalyst powder was dispersed in TA/NaOH solution (1:2, mol/mol), and this mixture was stirred for 1 h in the dark to blend well and allow the adsorption−desorption equilibrium before the irradiation of visible light. The suspension was magnetically stirred before and during the illumination. A 3 mL sample solution was drawn from the system at a certain time interval and analyzed by an Edinburgh FL/FS900 spectrophotometer. Electron spin resonance (ESR) signal of the radical species that are spin-trapped by 5,5-dimethyl-1-pyrroline-*N*-oxide (DMPO) was measured using a Bruker EPR A300 spectrometer. The irradiation source (λ > 420 nm) was a 300 W Xe arc lamp system, the very light source for our photocatalytic selective oxidation experiments as shown below.

The electrochemical analysis was carried out in a conventional three-electrode cell using a Pt plate and an Ag/AgCl electrode as the counter electrode and reference electrodes, respectively. The working electrode was prepared on fluoride−tin oxide (FTO) glass that was cleaned by sonication in ethanol for 30 min and dried at 353 K. The sample powder (10 mg) was ultrasonicated in 1 mL anhydrous ethanol to disperse it evenly to get slurry. The slurry was spreading onto FTO glass whose side part was previously protected using Scotch tape. The working electrode was dried overnight under ambient conditions. A copper wire was connected to the side part of the working electrode using a conductive tape. Uncoated parts of the electrode were isolated with epoxy resin. The exposed area of the working electrode was 0.25 cm^2. The visible light irradiation source was a 300 W Xe arc lamp system equipped with a UV cutoff filter (λ > 420 nm), the same light source as that for photoactivity test in the following. The photocurrent measurements were performed in homemade three electrode quartz cells with a PAR VMP3Multi Potentiotat apparatus. The electrolyte was 0.2 M aqueous Na_2SO_4 solution (pH 6.8) without additive. The electrochemical impedance spectroscopy (EIS) measurements were performed in the presence of 5.0 mM $K_3[Fe(CN)_6]/K_4[Fe(CN)_6]$ by applying an AC voltage with 5 mV amplitude in a frequency range from 1 Hz to 100 kHz under open circuit potential conditions.

Photoactivity. Aerobic selective oxidation of alcohols was performed using the similar reaction conditions to previous research works.[13,15,23−25,39] The only difference was to use deionized water as solvent herein instead of benzotrifluoride (BTF) as solvent. Typically, alcohol (0.1 mmol) and catalyst (8 mg) were dissolved in the solvent of deionized water (1.5 mL) saturated with pure molecular oxygen from a gas cyclinder.[15] This mixture was transferred into a 10 mL Pyrex glass bottle filled with molecular oxygen at a pressure of 0.1 MPa and stirred for half an hour to make the catalyst blend evenly in the solution. The suspensions were irradiated by a 300 W Xe arc lamp with a UV-CUT filter (λ > 420 nm). Controlled photoactivity experiments using different radicals scavengers (ammonium oxalate as scavenger for photogenerated holes,[13,15,40] *tert*-butyl alcohol as scavenger for hydroxyl radicals,[13,15,40,41] $AgNO_3$ as scavenger for electrons,[13,15,41,42] and benzoquinone as scavenger for superoxide radical species[13,15,43]) were performed similar to the above photocatalytic oxidation of alcohols except that radicals scavengers (0.1 mmol) were added to the reaction system.[13,15] After the reaction, the mixture was centrifuged to completely remove the catalyst particles. The remaining solution was analyzed based on an external standard method with a Shimadzu high performance liquid chromatograph (HPLC−LC20AT equipped with a C18 column and SPD-M20A

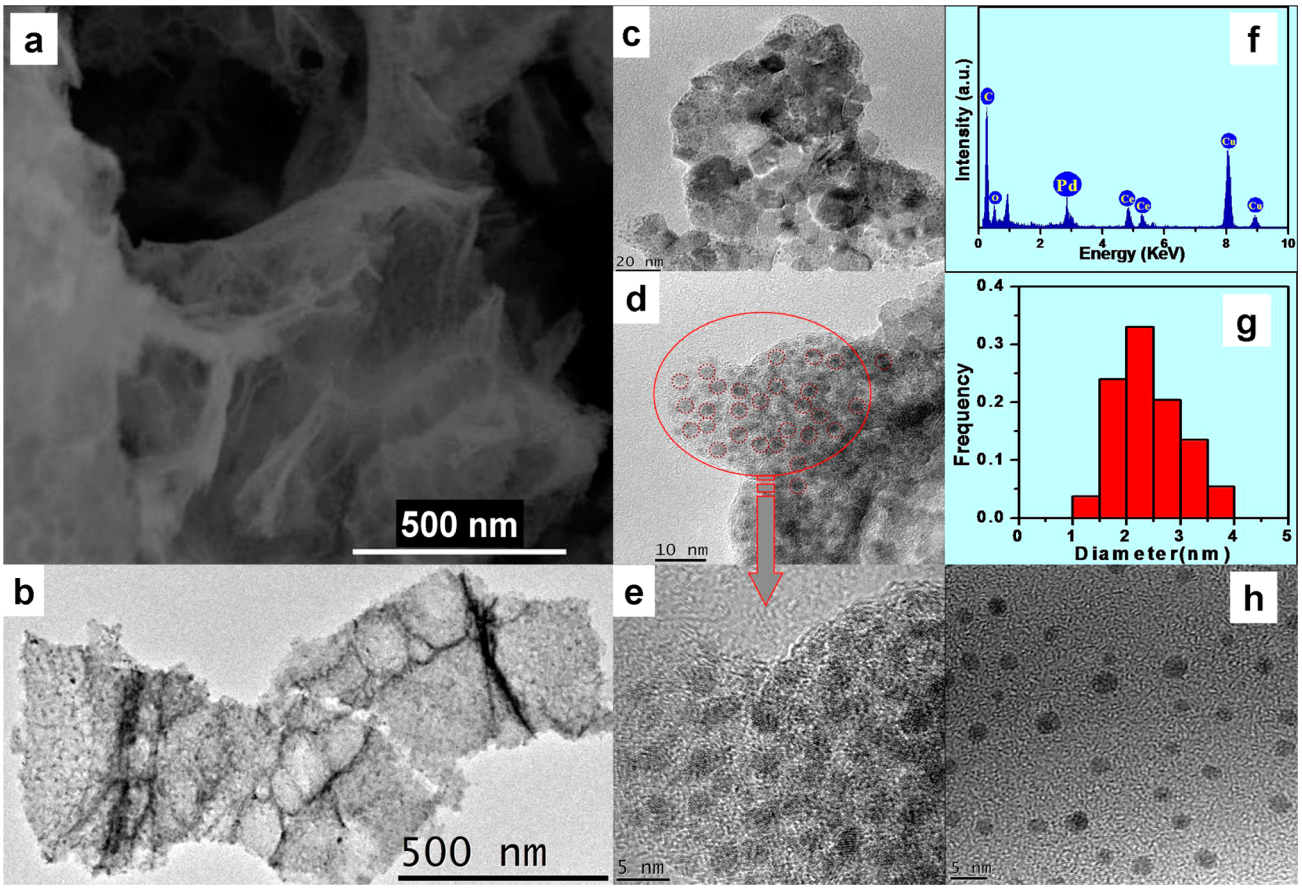

Figure 1. SEM (a), TEM (b, c) and HRTEM (d, e) images of the as-prepared Pd/CeO_2−NPs nanocomposite. EDX element analysis of Pd/CeO_2−NPs (f). Size distribution of Pd nanoparticles in Pd/CeO_2−NPs (g). Typical HRTEM image of original colloidal Pd nanoparticles (h).

photo diode array detector). Conversion and selectivity for oxidation of alcohols to target product aldehydes were defined as follows

$$\text{Conversion}\ (\%) = [(C_0 - C_r)/C_0] \times 100$$

$$\text{Selectivity}\ (\%) = [C_p/(C_0 - C_r)] \times 100$$

where C_0 is the initial concentration of alcohol, and C_r and C_p are the concentrations of reactant alcohol and product aldehyde, respectively, at a certain time after the photocatalytic reaction.

Anaerobic selective reduction of aromatic nitro-compounds was performed under N_2 bubbling with a flow rate of 40 mL/min. Typically, a 30 mg sample of photocatalyst and 30 mg of ammonium oxalate (as quenching agent for photogenerated holes to prevent oxidation reactions) were dispersed in 30 mL of deionized water by ultrasonication for 5 min. Then, a 30 mL of aqueous solution containing aromatic nitro-compounds (20 ppm) was added into the above suspension. The mixture was stirred for 1 h in the dark to blend well and allow the adsorption−desorption equilibrium before the irradiation by a 300 W Xe arc lamp with a UV-CUT filter (λ > 420 nm). After the reaction, the mixture was centrifuged to completely remove the catalyst particles. The remaining solution was analyzed with a Shimadzu high performance liquid chromatograph. Conversion and selectivity were defined similar to that for selective oxidation of alcohols.

■ RESULTS AND DISCUSSION

Figure 1 shows the typical scanning electron microscopy (SEM) and transmission electron microscopy (TEM) images of the Pd/CeO_2−NPs nanocomposite. It is shown in panels (a) and (b) that Pd/CeO_2−NPs has a silk "mat-like" structure. TEM analysis on the local area at a higher resolution (panel c) shows that this mat structure is composed by the tight accumulation of small nanoparticles of CeO_2−NPs support. The high-resolution TEM (HRTEM) analysis further evidences that on this mat structured CeO_2−NPs support tiny Pd nanoparticles can be distinguished clearly, as reflected by HRTEM images in panel (d) (red circled area) and (e). The energy dispersive X-ray (EDX) elements analysis evidences that the Pd/CeO_2−NPs nanocomposite is composed of Pd, Ce, and O, as shown in panel (f) of Figure 1. The size of Pd nanoparticles in Pd/CeO_2−NPs is in the range of 1−4 nm, as shown in panel (g) in Figure 1. Contrast comparison with the HRTEM image (panel h) of the original colloidal Pd nanoparticles suggests that the size and shape of Pd nanoparticles in Pd/CeO_2−NPs is nearly identical to those of the original colloidal Pd nanoparticles. Thus, it is clear that the calcination process at the high temperature (673 K) does not cause the aggregation of Pd nanoparticles on CeO_2−NPs.

The other important role of calcination process in air is to remove the protecting polyvinyllpyrrolidone (PVP) ligands in colloidal Pd nanoparticles on CeO_2−NPs, as confirmed by the X-ray photoelectron spectra (XPS) analysis on uncalcined Pd/CeO_2−NPs and calcined Pd/CeO_2−NPs, respectively. As shown in Figure 2, for uncalcined Pd/CeO_2−NPs, the N 1s signal is observed, which results from the PVP ligands of colloidal Pd nanoparticles. For calcined Pd/CeO_2−NPs, no N 1s signal is observed, suggesting that calcination in air at 673 K for 2 h is sufficient enough for the complete removal of PVP ligands from colloidal Pd nanoparticles. In addition, the Ce 3d XPS spectra show two peaks at around 881.6 and 899.9 eV

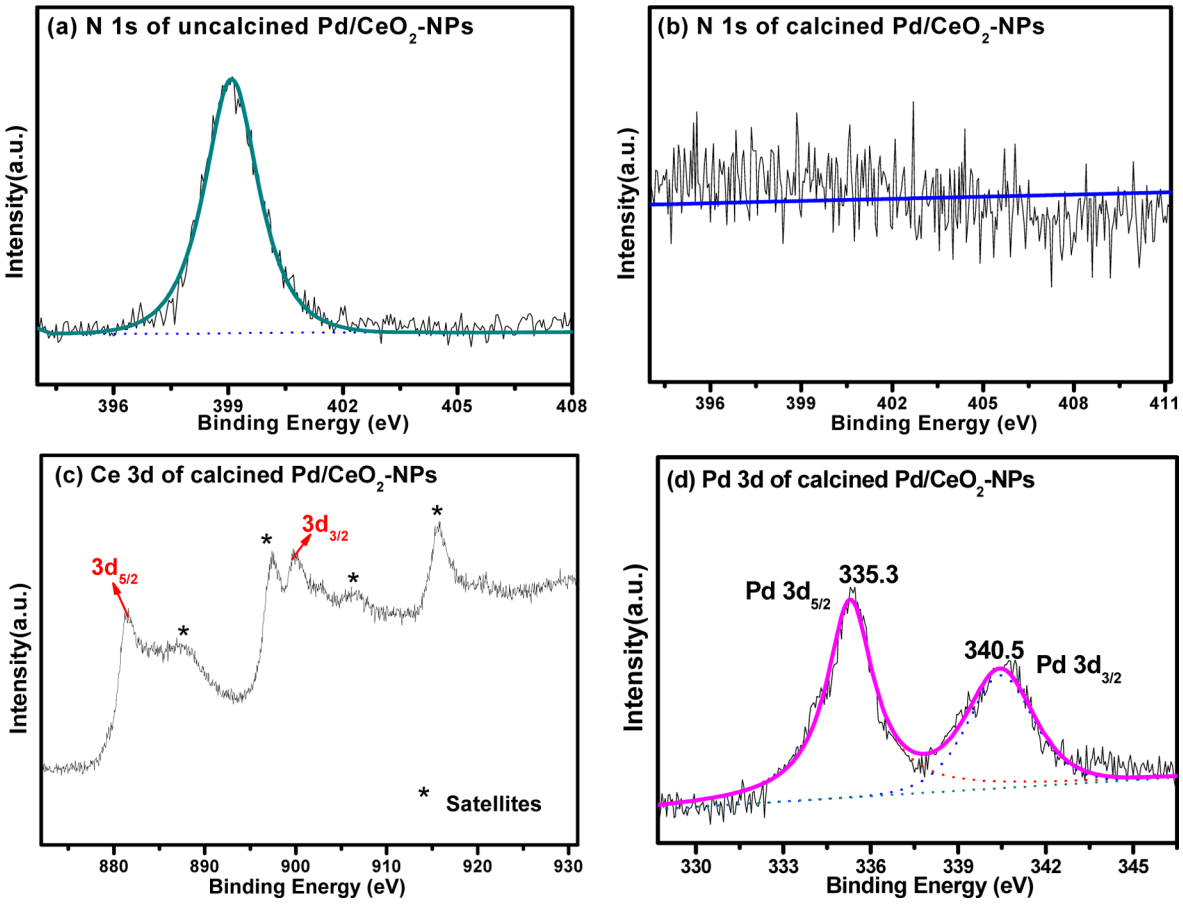

Figure 2. N 1s XPS spectra of uncalcined Pd/CeO_2−NPs (a) and calcined Pd/CeO_2−NPs (b). Ce 3d XPS (c) and Pd 3d XPS (d) spectra of calcined Pd/CeO_2−NPs.

corresponding to Ce $3d_{5/2}$ and Ce $3d_{3/2}$, respectively, and four satellite peaks indicated by asterisks, which indicate that the valence state of Ce in calcined Pd/CeO_2−NPs is +4.[44,45] The peaks located at 335.3 and 340.5 eV in Pd 3d XPS spectra are ascribed to the $3d_{5/2}$ and $3d_{3/2}$ of metallic Pd, respectively.[46]

To understand the key importance of the support effect on the as-formed morphology and aggregation inhibition of tiny Pd nanoparticles, we have used the same preparation procedures to synthesize Pd nanoparticles supported on commercial CeO_2, i.e., Pd/commercial CeO_2, by replacing the nanosized CeO_2 support with commercial CeO_2 powder. It is clear from the typical TEM and SEM images in Figures S1 and S2 of the Supporting Information that (i) the morphology of Pd/commercial CeO_2 is remarkably different from Pd/CeO_2−NPs and (ii) significant aggregation of tiny Pd nanoparticles is obviously observed. Therefore, the use of nanosized CeO_2 support is an important factor driving the formation of such a unique mat morphology and inhibiting the aggregation of tiny Pd nanoparticles. The latter effect can also be indirectly reflected by the UV−visible diffuse reflectance spectra (DRS) of Pd/CeO_2−NPs and Pd/commercial CeO_2. As shown in Figure 3, the anchoring of Pd nanoparticles onto commercial CeO_2 and nanosized CeO_2−NPs support leads to the increase in visible light absorption. However, notably, for Pd/commercial CeO_2, a small peak around 500 nm appears, which is distinctly different from that for Pd/CeO_2−NPs. This peak cannot be attributed to the plasmon-induced light absorption of metal Pd because unlike Au or Ag nanoparticles[47] there are no typical surface plasmon resonance (SPR) peaks for

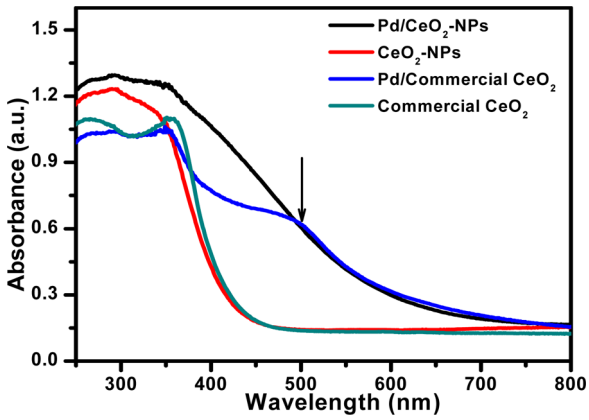

Figure 3. UV−visible diffuse reflectance spectra (DRS) of Pd/CeO_2−NPs, Pd/commercial CeO_2, bare support of CeO_2−NPs, and commercial CeO_2.

Pd nanoparticles in the visible light region.[10] The peak at around 500 nm is due to the aggregation of Pd nanoparticles, and such a similar phenomenon is also observed in the previous study.[48] The other useful information from the DRS spectra in Figure 3 is that the band edge of CeO_2 support suggests that the visible light irradiation (λ > 420 nm) can induce "band-gap-photoexcitation" of semiconductor CeO_2,[49] thus forming electron−hole pairs. As a result, these samples could potentially be used as a visible light photocatalyst for specific oxidative or reductive reactions. In particular, the unique remarkable

Table 1. Selective Oxidation of Various Alcohols in Water Over Pd/CeO_2−NPs and Pd/Commercial CeO_2 Under Visible Light Irradiation (λ > 420 nm) for 4 h at Room Temperature[a]

Substrate	Product	Conversion (%)	Selectivity (%)
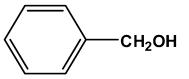	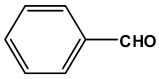	91 (7)	99 (98)
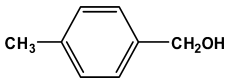	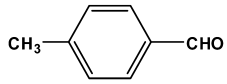	69 (6)	97 (96)
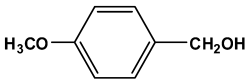		62 (6)	98 (98)
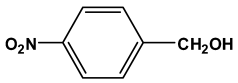	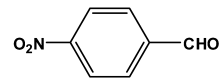	67 (5)	96 (95)
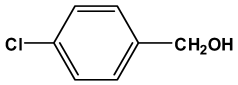	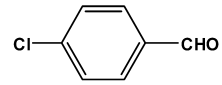	59 (7)	96 (95)
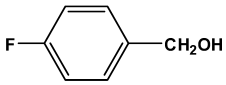	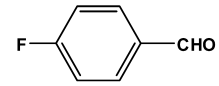	58 (8)	92 (91)
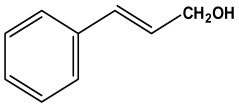	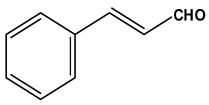	54 (7)	81 (79)
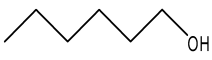		21 (3)	100 (100)
		21 (3)	100 (100)

[a]The data in parentheses are conversion and selectivity over Pd/commercial CeO_2 under identical reaction conditions.

morphology as well as the structure composition of Pd/CeO_2−NPs could probably lead to the distinctive "morphology-dependent" photocatalytic performance.

We have then benchmarked the photocatalytic performance of these samples toward aerobic oxidation of alcohols in water, a key transformation in synthesis of fine chemicals because carbonyl compounds (e.g., aldehydes) are important intermediates in the fragrance, confectionary, and pharmaceutical industries.[16,17,23−27] As shown in Table 1, Pd/CeO_2−NPs has significantly higher photoactivity than Pd/commercial CeO_2. In terms of the yield ratio of aldehydes, the photoactivity of Pd/CeO_2−NPs is about 7−13 times higher than that of Pd/commercial CeO_2. In addition, it is worth noting that the oxidation of benzylic alcohols shows a much higher conversion than that for aliphatic alcohols, which could be ascribed to the fact that the β-hydrogen atom in benzylic alcohols is more active. The different photoactivity also suggests that photocatalytic oxidation of aromatic alcohols and aliphatic alcohols to corresponding aldehydes over Pd/CeO_2−NPs might show a different stereoselective chemistry.[25] Importantly, it should be noted that even if we prolong the visible light irradiation time to 8 h for the oxidation of alcohols over Pd/commercial CeO_2, the conversion is only slightly increased by 2−3% but with a decrease in selectivity to aldehydes, which suggests that Pd/commercial CeO_2 is a very low active visible light photocatalyst for selective oxidation of alcohols compared to the highly photoactive and selective Pd/CeO_2−NPs with a unique structural and morphological composition. Controlled experiments using bare CeO_2−NPs or commercial CeO_2 support indicate that the very low yield is obtained under identical reaction conditions (Figure S3, Supporting Information), which suggests the importance of Pd loading on improving the photoactivity of CeO_2. This is understandable because noble metal nanoparticles are well-known electron reservoirs for photocatalysts consisting of noble metal nanoparticles supported on semiconductors.[47,50,51] Therefore, under visible light irradiation, the Pd nanoparticles are able to capture photogenerated electrons from semiconductor CeO_2 support, prolonging the lifetime of electron−hole pairs and thus enhancing the photoactivity of Pd/CeO_2−NPs or Pd/commercial CeO_2. However, notably, the photoactivity improvement due to Pd loading onto CeO_2−NPs is much higher than that of Pd/commercial CeO_2. Such a significant photoactivity enhancement for Pd/CeO_2−NPs should be attributed to the influence of its specific morphology and structure composition as compared to Pd/commercial CeO_2. As shown in Figure 4a, under visible light irradiation, the photocurrent intensity for Pd/CeO_2−NPs is much higher than that of Pd/commercial CeO_2, suggesting a longer lifetime of charge carriers photogenerated over Pd/CeO_2−NPs than Pd/commercial CeO_2, which is in good agreement with the photoluminescence (PL) spectra (Figure S4, Supporting Information). Figure 4b shows the electrochemical impedance spectroscopy (EIS) Nyquist plots of the electrode samples of Pd/CeO_2−NPs and Pd/commercial CeO_2, which show that Pd/CeO_2−NPs has a much smaller arc than Pd/commercial CeO_2, suggesting the more efficient transfer of charge carriers over the surface of Pd/CeO_2−NPs. The longer lifetime of

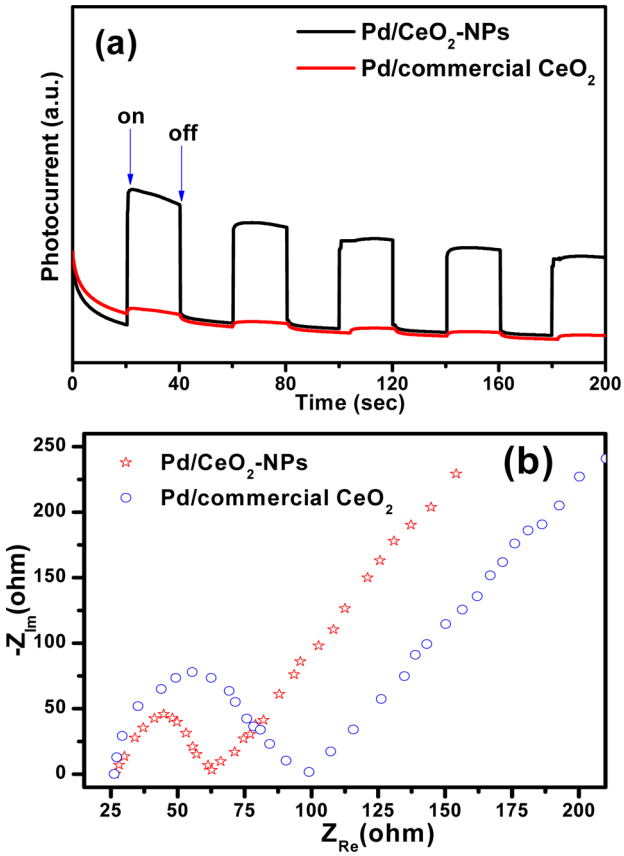

Figure 4. Photocurrent transient response (a) and electrochemical impedance spectroscopy Nyquist plots (b) of the sample electrodes of Pd/CeO_2−NPs and Pd/commercial CeO_2 under visible light irradiation.

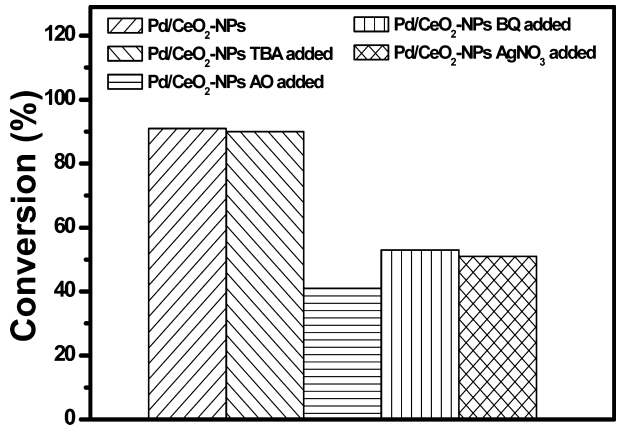

Figure 5. Controlled experiments using different radicals scavengers: *tert*-butyl alcohol (TBA) for hydroxyl radicals, ammonium oxalate (AO) for holes, benzoquinone (BQ) for superoxide radicals, and $AgNO_3$ for electrons for oxidation of benzyl alcohol in the solvent of water over Pd/CeO_2−NPs under visible light irradiation for 4 h.

photogenerated charge carriers and more efficient charge transfer over Pd/CeO_2−NPs are largely beneficial for improving visible light photoactivity toward aerobic oxidation of alcohols.

As mentioned above, there is no SPR peak for Pd nanoparticles in the visible light region. For Pd/commercial CeO_2, the small peak at about 500 nm in the DRS spectra in Figure 3 is due to the aggregation of Pd nanoparticles. Only trace conversion of alcohols is obtained by wavelength-selective (with a 500 ± 15 nm band-pass filter) visible light irradiation for 4 h. Therefore, the SPR-induced photoactivity contribution can be ruled out for Pd/CeO_2−NPs and Pd/commercial CeO_2, and the role of Pd nanoparticles mainly acts as an electron reservoir to capture photogenerated electrons from semiconductor CeO_2 to lengthen the fate of photogenerated electron−hole (e^-−h^+) pairs, which is distinctly different from plasmonic Au photocatalyst for aerobic oxidation of alcohols.[35,36]

To gain further insight into the reaction mechanism, we have performed a series of controlled experiments. Initial blank experiments in the absence of photocatalysts and/or visible light show no or trace conversion of alcohols, confirming that the reaction is really driven by a photocatalytic process. Experiments in inert nitrogen atmosphere show trace conversion of alcohols, confirming that oxygen is the primary oxidant. Controlled experiments using different radicals scavengers offer more insightful information on the role of photogenerated radical species.[13,15,23,52] As shown in Figure 5, when the scavenger ammonium oxalate (AO) for holes is added, conversion of benzyl alcohol is significantly prohibited. When the scavenger benzoquinone (BQ) for superoxide radicals or scavenger $AgNO_3$ for electrons is added, conversion of benzyl alcohol is also decreased remarkably. However, the addition of scavenger *tert*-butyl alcohol (TBA) for hydroxyl radicals into reaction system plays a negligible effect on conversion of benzyl alcohol; a similar phenomenon is also observed for other alcohols (Figures S5 and S6, Supporting Information). The presence of superoxide radicals is confirmed by ESR spectra (Figure S8, Supporting Information), while the hydroxyl radicals are confirmed by both ESR spectra and •OH-trapping fluorescence spectra (Figures S7 and S8, Supporting Information). The above results suggest that for aerobic oxidation of alcohols in water over Pd/CeO_2−NPs under visible light irradiation the positive holes, oxygen, or superoxide radicals play important roles instead of hydroxyl radicals. The observation of the negligible role of hydroxyl radicals on aerobic oxidation of alcohols in water over Pd/CeO_2−NPs is quite interesting because this observation suggests that in order to achieve high selectivity for photocatalytic aerobic oxidation of alcohols to aldehydes over semiconductor-based photocatalysts it is not the necessary requisite to avoid the generation of the so-called "nonselective" hydroxyl radicals.[17,24] In fact, the high selectivity obtained in water over Pd/CeO_2−NPs and Pd/commercial CeO_2 under visible light irradiation is very similar to that (Table S1, Supporting Information) obtained in organic solvent of benzotrifluoride (BTF) in which no hydroxyl radicals are generated.[13,24,25,33] Our results suggest that the selectivity to aldehydes is not affected in a considerable way by the presence of hydroxyl radicals for aerobic oxidation of alcohols in water over the current Pd/CeO_2−NPs under visible light irradiation.

Previously, Palmisano's group investigated the photocatalytic performance of TiO_2 with different phase, crystallinity, and morphology toward aerobic oxidation of aromatic alcohols to aldehydes in water under UV light irradiation.[17] They found that a rutile TiO_2 with bad crystallinity has the highest selectivity of 60% at a conversion of 50%. Their work indicates that in the presence of photogenerated holes and hydroxyl radicals for TiO_2 in water other structural parameters also play synergetic roles in affecting selectivity.[17] Our current findings strongly suggest that the appropriate choice of semiconductors,

Table 2. Selective Reduction of Various Aromatic Nitro-Compounds in Water over Pd/CeO_2−NPs and Pd/Commercial CeO_2 under Visible Light Irradiation (λ > 420 nm) for 4 h at Room Temperature[a]

Substrate	Product	Conversion (%)	Selectivity (%)
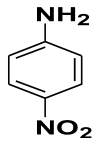	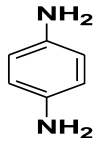	95 (61)	98 (98)
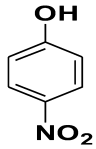	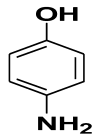	99 (51)	96 (96)
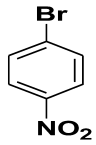	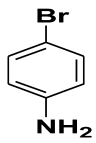	71 (34)	98 (97)
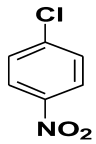	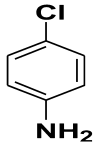	78 (41)	97 (96)
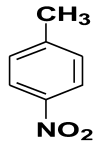	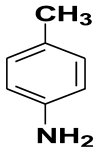	75 (38)	98 (98)
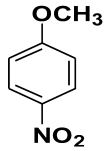	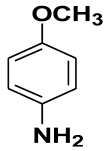	72 (39)	97 (97)

[a]The data in parentheses are conversion and selectivity over Pd/commercial CeO_2 under identical reaction conditions.

besides TiO_2, coupled with constructing specific structure composition and morphology can offer a very promising way to achieve high selectivity and activity for photocatalytic aerobic oxidation of alcohols to aldehydes in water under visible light irradiation. Importantly, it is not necessary to avoid the presence of hydroxyl radicals and holes in order to achieve the high selectivity for semiconductor-based photocatalytic selective oxidation of alcohols; on the contrary, the choice of proper semiconductors via constructing specific structure and morphology is able to promote aerobic oxidation of alcohols with high selectivity in water, a green solvent in photocatalysis.[17]

The other factor affecting the photoactivity is the surface area of samples. As shown in Figure S9 of the Supporting Information, the surface area of Pd/CeO_2−NPs is about 145 m^2/g, much higher than 24 m^2/g for Pd/commercial CeO_2. The higher surface area results in larger adsorption capacity toward alcohols, as ascertained by the adsorption measurement (Figure S10, Supporting Information). However, note that the photoactivity of bare CeO_2−NPs support is lower than Pd/commercial CeO_2 (Figure S3, Supporting Information), although the surface area of CeO_2−NPs is much higher than that of Pd/commercial CeO_2 (Figure S9, Supporting Information). This indicates that the surface area is not the only primary factor accounting for the much higher photoactivity of Pd/CeO_2−NPs than those of Pd/commercial CeO_2, bare CeO_2−NPs, and commercial CeO_2.

In addition to the high visible light photoactivity and selectivity toward aerobic oxidation of alcohols in water, the nanoassembly of Pd/CeO_2−NPs can also exhibit improved efficiency in anaerobic selective reduction of aromatic nitro-compounds to corresponding aromatic amines, which represents one significant chemical transformation in synthetic organic chemistry[53] in water under visible light irradiation as compared to Pd/commercial CeO_2. Because Pd/CeO_2−NPs has the enhanced lifetime of photogenerated electron−hole pairs, the more accessible photogenerated electrons could drive the reduction reaction more efficiently, while the positive holes with oxidative power is quenched by adding ammonium oxalate, and the reaction is performed under nitrogen atmosphere instead of oxygen atmosphere. This inference is faithfully ascertained by the higher photoactivity of Pd/CeO_2−NPs than that of Pd/commercial CeO_2 toward anaerobic selective reduction of nitro-compounds to corresponding amines as shown in Table 2. Controlled experiments by adding $AgNO_3$ as the quenching agent for photogenerated electrons in

the reaction system show that the reaction for reduction of aromatic nitro-compounds hardly occurs, which clearly suggests that the anaerobic selective reduction of aromatic nitro-compounds in water is driven by the photogenerated electrons over Pd/CeO_2−NPs or Pd/commercial CeO_2 under visible light irradiation.

In summary, we have reported the synthesis of Pd/CeO_2−NPs featuring a dispersion of tiny metallic Pd nanoparticles on the CeO_2−NPs support with a unique mat morphology that is able to act as a highly selective visible light-driven photocatalyst toward photoredox transformations, including aerobic oxidation of alcohols and anaerobic reduction of nitro-compounds in water under ambient conditions. The high photoactivity can be attributed to the integrative factors, unique mat structure and morphological composition, improved lifetime and transfer of charge carriers, and higher surface area of Pd/CeO_2−NPs. This work expands the new type of visible light semiconductor photocatalyst toward "green" chemistry-oriented selective organic transformations in the green solvent of water[54,55] under ambient conditions.

■ ASSOCIATED CONTENT

Supporting Information

Typical TEM and SEM images of Pd/commercial CeO_2, controlled experiments using the bare CeO_2 nanoparticles (CeO_2−NPs) and commercial CeO_2 for oxidation of alcohols, photoluminescence (PL) spectra of the samples of Pd/CeO_2−NPs, Pd/commercial CeO_2 and the bare support of commercial CeO_2 and CeO_2−NPs, controlled experiments using different radicals scavengers for oxidation of cinnamyl alcohol and n-hexanol in water over Pd/CeO_2−NPs, electron spin resonance (ESR) spectra of superoxide radicals and hydroxyl radicals trapped by DMPO over the suspensions of Pd/CeO_2−NPs and Pd/commercial CeO_2, time-dependent •OH-trapping fluorescence spectra by the reaction of terephthalic acid (TA) with the •OH radicals photogenerated by the Pd/CeO_2−NPs photocatalyst in an aqueous phase under visible light irradiation, selective oxidation of various alcohols in organic solvent of benzotrifluoride (BTF) over Pd/CeO_2−NPs and Pd/commercial CeO_2 under visible light irradiation, nitrogen adsorption−desorption isotherms of the samples of Pd/CeO_2−NPs and Pd/commercial CeO_2, adsorption capacity of Pd/CeO_2−NPs and Pd/commercial CeO_2 toward substrate alcohols, and appendix for samples photographs. This material is available free of charge via the Internet at http://pubs.acs.org.

■ AUTHOR INFORMATION

Corresponding Author

*Tel./Fax: +86 591 83779326. E-mail: yjxu@fzu.edu.cn.

Notes

The authors declare no competing financial interest.

■ ACKNOWLEDGMENTS

The support by the National Natural Science Foundation of China (NSFC) (21173045, 20903022, 20903023), Award Program for Minjiang Scholar Professorship, Natural Science Foundation (NSF) of Fujian Province for Distinguished Young Investigator Grant (2012J06003), Program for Changjiang Scholars and Innovative Research Team in Universities (PCSIRT0818), Program for Returned High-Level Overseas Chinese Scholars of Fujian Province, and Project Sponsored by the Scientific Research Foundation for the Returned Overseas Chinese Scholars, State Education Ministry, is gratefully acknowledged.

■ REFERENCES

(1) Fox, M. A.; Dulay, M. T. Heterogeneous photocatalysis. *Chem. Rev.* **1993**, *93*, 341−357.
(2) Hoffmann, M. R.; Martin, S. T.; Choi, W.; Bahnemann, D. W. Environmental applications of semiconductor photocatalysis. *Chem. Rev.* **1995**, *95*, 69−96.
(3) Linsebigler, A. L.; Lu, G.; Yates, J. T. Photocatalysis on TiO_2 surface: Principles, mechanisms, and selected results. *Chem. Rev.* **1995**, *95*, 735−758.
(4) Mills, A.; Le Hunte, S. An overview of semiconductor photocatalysis. *J. Photochem. Photobiol., A* **1997**, *108*, 1−35.
(5) Fujishima, A.; Rao, T. N.; Tryk, D. A. Titanium dioxide photocatalysis. *J. Photochem. Photobiol., C* **2000**, *1*, 1−21.
(6) Zhang, Z.; Yates, J. T., Jr. Band bending in semiconductors: Chemical and physical consequences at surfaces and interfaces. *Chem. Rev.* **2012**, *112*, 5520−5551.
(7) Cheng, W.-Y.; Chen, W.-T.; Hsu, Y.-J.; Lu, S.-Y. Modulation and improvement on separation of photoinduced charge carriers in CdS−metal nanoheterostructures. *J. Phys. Chem. C* **2009**, *113*, 17342−17346.
(8) Kamat, P. V. Manipulation of charge transfer across semiconductor interface. A criterion that cannot be ignored in photocatalyst design. *J. Phys. Chem. Lett.* **2012**, *3*, 663−672.
(9) Liu, S.; Zhang, N.; Tang, Z.-R.; Xu, Y.-J. Synthesis of one-dimensional CdS@TiO_2 core−shell nanocomposites photocatalyst for selective redox: The dual role of TiO_2 shell. *ACS Appl. Mater. Interfaces* **2012**, *4*, 6378−6385.
(10) Zhang, N.; Liu, S.; Fu, X.; Xu, Y.-J. Synthesis of M@TiO_2 (M = Au, Pd, Pt) core−shell nanocomposites with tunable photoreactivity. *J. Phys. Chem. C* **2011**, *115*, 9136−9145.
(11) Zeng, H. C. Integrated nanocatalysts. *Acc. Chem. Res.* **2013**, *46*, 226−235 and references therein..
(12) Zhou, K.; Li, Y. Catalysis based on nanocrystals with well-defined facets. *Angew. Chem., Int. Ed.* **2012**, *51*, 602−613.
(13) Zhang, Y.; Zhang, N.; Tang, Z.-R.; Xu, Y.-J. Transforming CdS into an efficient visible light photocatalyst for selective oxidation of saturated primary C−H bonds under ambient conditions. *Chem. Sci.* **2012**, *3*, 2812−2822.
(14) Yang, H. G.; Sun, C. H.; Qiao, S. Z.; Zou, J.; Liu, G.; Smith, S. C.; Cheng, H. M.; Lu, G. Q. Anatase TiO_2 single crystals with a large percentage of reactive facets. *Nature* **2008**, *453*, 638−641.
(15) Zhang, Y.; Zhang, N.; Tang, Z.-R.; Xu, Y.-J. Identification of Bi_2WO_6 as a highly selective visible-light photocatalyst toward oxidation of glycerol to dihydroxyacetone in water. *Chem. Sci.* **2013**, *4*, 1820−1824.
(16) Zhang, N.; Zhang, Y.; Pan, X.; Fu, X.; Liu, S.; Xu, Y.-J. Assembly of CdS nanoparticles on the two-dimensional graphene scaffold as visible-light-driven photocatalyst for selective organic transformation under ambient conditions. *J. Phys. Chem. C* **2011**, *115*, 23501−23511.
(17) Yurdakal, S.; Palmisano, G.; Loddo, V.; Augugliaro, V.; Palmisano, L. Nanostructured rutile TiO_2 for selective photocatalytic oxidation of aromatic alcohols to aldehydes in water. *J. Am. Chem. Soc.* **2008**, *130*, 1568−1569.
(18) Burda, C.; Chen, X.; Narayanan, R.; El-Sayed, M. A. Chemistry and properties of nanocrystals of different shapes. *Chem. Rev.* **2005**, *105*, 1025−1102.
(19) Chen, X.; Mao, S. S. Titanium dioxide nanomaterials: Synthesis, properties, modifications, and applications. *Chem. Rev.* **2007**, *107*, 2891−2959.
(20) Li, Y.-F.; Liu, Z.-P. Particle size, shape and activity for photocatalysis on titania anatase nanoparticles in aqueous surroundings. *J. Am. Chem. Soc.* **2011**, *133*, 15743−15752.
(21) Zaera, F. The new materials science of catalysis: Toward controlling selectivity by designing the structure of the active site. *J. Phys. Chem. Lett.* **2010**, *1*, 621−627.

(22) Wang, X.; Caruso, R. A. Enhancing photocatalytic activity of titania materials by using porous structures and the addition of gold nanoparticles. *J. Mater. Chem.* **2011**, *21*, 20−28.
(23) Zhang, N.; Zhang, Y.; Yang, M. Q.; Tang, Z.-R.; Xu, Y.-J. A critical and benchmark comparison on graphene-, carbon nanotube-, and fullerene-semiconductor nanocomposites as visible light photocatalysts for selective oxidation. *J. Catal.* **2013**, *453*, 181−187.
(24) Zhang, M.; Chen, C.; Ma, W.; Zhao, J. Visible-light-induced aerobic oxidation of alcohols in a coupled photocatalytic system of dye-sensitized TiO_2 and TEMPO. *Angew. Chem., Int. Ed.* **2008**, *47*, 9730−9733.
(25) Zhang, Y.; Tang, Z.-R.; Fu, X.; Xu, Y.-J. Engineering the unique 2D mat of graphene to achieve graphene-TiO_2 nanocomposite for photocatalytic selective transformation: What advantage does graphene have over its forebear carbon nanotube? *ACS Nano* **2011**, *5*, 7426−7435.
(26) Zhang, M.; Wang, Q.; Chen, C.; Zang, L.; Ma, W.; Zhao, J. Oxygen atom transfer in the photocatalytic oxidation of alcohols by TiO_2: Oxygen isotope studies. *Angew. Chem., Int. Ed.* **2009**, *48*, 6081−6084.
(27) Enache, D. I.; Edwards, J. K.; Landon, P.; Solsona-Espriu, B.; Carley, A. F.; Herzing, A. A.; Watanabe, M.; Kiely, C. J.; Knight, D. W.; Hutchings, G. J. Solvent-free oxidation of primary alcohols to aldehydes using Au-Pd/TiO_2 catalysts. *Science* **2006**, *311*, 362−365.
(28) Zhang, N.; Zhang, Y.; Pan, X.; Fu, X.; Xu, Y.-J. Research progress on photocatalytic selective oxidation and reduction in organic synthesis. *Sci. China Chem.* **2011**, *41*, 1097−1111.
(29) Palmisano, G.; Augugliaro, V.; Pagliaro, M.; Palmisano, L. Photocatalysis: A promising route for 21st century organic chemistry. *Chem. Commun.* **2007**, 3425−3437.
(30) Maldotti, A.; Molinari, A.; Amadelli, R. Photocatalysis with organized systems for the oxofunctionalization of hydrocarbons by O_2. *Chem. Rev.* **2002**, *102*, 3811−3836.
(31) Shiraishi, Y.; Hirai, T. Selective organic transformations on titanium oxide-based photocatalysts. *J. Photochem. Photobiol., C* **2008**, *9*, 157−170.
(32) Palmisano, G.; Garcia-Lopez, E.; Marci, G.; Loddo, V.; Yurdakal, S.; Augugliaro, V.; Palmisano, L. Advances in selective conversions by heterogeneous photocatalysis. *Chem. Commun.* **2010**, *46*, 7074−7089.
(33) Wang, Q.; Zhang, M.; Chen, C.; Ma, W.; Zhao, J. Photocatalytic aerobic oxidation of alcohols on TiO_2: The acceleration effect of a bronsted acid. *Angew. Chem., Int. Ed.* **2010**, *49*, 7976−7979.
(34) Naya, S.-i.; Inoue, A.; Tada, H. Self-assembled heterosupramolecular visible light photocatalyst consisting of gold nanoparticle-loaded titanium (IV) dioxide and surfactant. *J. Am. Chem. Soc.* **2010**, *132*, 6292−6293.
(35) Tsukamoto, D.; Shiraishi, Y.; Sugano, Y.; Ichikawa, S.; Tanaka, S.; Hirai, T. Gold nanoparticles located at the interface of anatase/rutile TiO_2 particles as active plasmonic photocatalysts for aerobic oxidation. *J. Am. Chem. Soc.* **2012**, *134*, 6309−6315.
(36) Tanaka, A.; Hashimoto, K.; Kominami, H. Preparation of Au/CeO_2 exhibiting strong surface plasmon resonance effective for selective or chemoselective oxidation of alcohols to aldehydes or ketones in aqueous suspensions under irradiation by green light. *J. Am. Chem. Soc.* **2012**, *134*, 14526−14533.
(37) Narayanan, R.; El-Sayed, M. A. Effect of catalysis on the stability of metallic nanoparticles: Suzuki reaction catalyzed by PVP-palladium nanoparticles. *J. Am. Chem. Soc.* **2003**, *125*, 8340−8347.
(38) Teranishi, T.; Miyake, M. Size control of palladium nanoparticles and their crystal structures. *Chem. Mater.* **1998**, *10*, 594−600.
(39) Zhang, N.; Liu, S.; Fu, X.; Xu, Y.-J. A simple strategy for fabrication of "plum-pudding" type Pd@CeO_2 semiconductor nanocomposite as a visible-light-driven photocatalyst for selective oxidation. *J. Phys. Chem. C* **2011**, *115*, 22901−22909.
(40) Carp, O.; Huisman, C. L.; Reller, A. Photoinduced reactivity of titanium dioxide. *Prog. Solid State Chem.* **2004**, *32*, 33−177.
(41) Yang, M. Q.; Zhang, N.; Xu, Y.-J. Synthesis of fullerene−, carbon nanotube− and graphene−TiO_2 nanocomposite photocatalysts for selective oxidation. A comparative study. *ACS Appl. Mater. Interfaces* **2013**, *5*, 1156−1164.
(42) Primo, A.; Marino, T.; Corma, A.; Molinari, R.; García, H. Efficient visible-light photocatalytic water splitting by minute amounts of gold supported on nanoparticulate CeO_2 obtained by a biopolymer templating method. *J. Am. Chem. Soc.* **2011**, *133*, 6930−6933.
(43) Stylidi, M.; Kondarides, D. I.; Verykios, X. E. Visible light-induced photocatalytic degradation of acid orange 7 in aqueous TiO_2 suspensions. *Appl. Catal., B* **2004**, *47*, 189−201.
(44) Schierbaum, K.-D. Ordered ultra-thin cerium oxide overlayers on Pt(111) single crystal surfaces studied by LEED and XPS. *Surf. Sci.* **1998**, *399*, 29−38.
(45) Bera, P.; Priolkar, K. R.; Gayen, A.; Sarode, P. R.; Hegde, M. S.; Emura, S.; Kumashiro, R.; Jayaram, V.; Subbanna, G. N. Ionic dispersion of Pt over CeO_2 by the combustion method: structural investigation by XRD, TEM, XPS, and EXAFS. *Chem. Mater.* **2003**, *15*, 2049−2060.
(46) Priolkar, K. R.; Bera, P.; Sarode, P. R.; Hegde, M. S.; Emura, S.; Kumashiro, R.; Lalla, N. P. formation of $Ce_{1-x}Pd_xO_{2-\delta}$ solid solution in combustion-synthesized Pd/CeO_2 catalyst: XRD, XPS, and EXAFS investigation. *Chem. Mater.* **2002**, *14*, 2120−2128.
(47) Kamat, P. V. Photophysical, photochemical and photocatalytic aspects of metal nanoparticles. *J. Phys. Chem. B* **2002**, *106*, 7729−7744.
(48) Xiong, Y.; Chen, J.; Wiley, B.; Xia, Y.; Yin, Y.; Li, Z.-Y. Size-dependence of surface plasmon resonance and oxidation for Pd nanocubes synthesized via a seed etching process. *Nano Lett.* **2005**, *5*, 1237−1242.
(49) Zhang, N.; Fu, X.; Xu, Y.-J. A facile and green approach to synthesize Pt@CeO_2 nanocomposite with tunable core−shell and yolk−shell structure and its application as a visible light photocatalyst. *J. Mater. Chem.* **2011**, *21*, 8152−8158.
(50) Hirakawa, T.; Kamat, P. V. Charge separation and catalytic activity of Ag@TiO_2 core−shell composite clusters under UV−irradiation. *J. Am. Chem. Soc.* **2005**, *127*, 3928−3934.
(51) Maeda, K.; Domen, K. Photocatalytic water splitting: Recent progress and future challenges. *J. Phys. Chem. Lett.* **2010**, *1*, 2655−2661.
(52) Zhang, Y.; Zhang, N.; Tang, Z.-R.; Xu, Y.-J. Graphene transforms wide band Gap ZnS to a visible light photocatalyst. The new role of graphene as a macromolecular photosensitizer. *ACS Nano* **2012**, *6*, 9777−9789.
(53) Zhang, N.; Xu, Y.-J. Aggregation- and leaching-resistant, reusable, and multifunctional Pd@CeO_2 as a robust nanocatalyst achieved by a hollow core−shell strategy. *Chem. Mater.* **2013**, *25*, 1979−1988.
(54) Simon, M.-O.; Li, C.-J. Green chemistry oriented organic synthesis in water. *Chem. Soc. Rev.* **2012**, *41*, 1415−1427.
(55) Ten Brink, G.-J.; Arends, I. W. C. E.; Sheldon, R. A. Green, catalytic oxidation of alcohols in water. *Science* **2000**, *287*, 1636−1639.